Journal of Extracellular Vesicles

RESEARCH ARTICLE OPEN ACCESS

Extracellular Vesicles Define Discrete Nano-Based Niches Within the Human Haematopoietic System

Isabelle J. Grenier-Pleau[1] | Christopher J. Wells[1] | Samantha M. Holmes[1] | Christine Hall[1] | Michael Vermeulen[2] | Camille A. de Villiers[3,4] | Jelle Penders[3] | Simon Vilms Pedersen[5] | Sarah A. Dick[1] | Eric Bonneil[6] | Mykhaylo Slobodyanyuk[7] | Murtaza S. Nagree[8] | Jasleen Kaur[1] | Amy J. M. McNaughton[9] | Jamie Beaulieu[6] | Molly M. Stevens[4,10] | Stephanie Z. Xie[8] | Michael J. Rauh[9] | Lynne-Marie Postovit[1] | David J. H. F. Knapp[6] | Jüri Reimand[7,11] | Kathrin Tyryshkin[9] | Pierre Thibault[6] | Andrew W. Craig[1] | John F. Rudan[12] | Steve Mann[12] | Edmond Y. W. Chan[1] | Sheela A. Abraham[1]

[1]Department of Biomedical and Molecular Sciences, Queen's University, Kingston, Ontario, Canada | [2]Department of Biology, Queen's University, Kingston, Ontario, Canada | [3]SPARTA Biodiscovery, London, UK | [4]Department of Materials, Department of Bioengineering, Institute for Biomedical Engineering, Imperial College London, London, UK | [5]Department of Green Technology, University of Southern Denmark, Odense, Denmark | [6]Institute for Research in Immunology and Cancer, Université de Montréal, Montréal, Quebec, Canada | [7]Computational Biology Program, Ontario Institute for Cancer Research, 661 University Ave Suite 510 and Department of Medical Biophysics, University of Toronto, Toronto, Ontario, Canada | [8]Princess Margaret Cancer Centre, University Health Network, Toronto, Ontario, Canada | [9]Department of Pathology and Molecular Medicine, Queen's University, Kingston, Ontario, Canada | [10]Department of Physiology, Anatomy and Genetics, Department of Engineering Science, Kavli Institute for Nanoscience Discovery, University of Oxford, Oxford, UK | [11]Department of Molecular Genetics, University of Toronto, Toronto, Ontario, Canada | [12]Department of Surgery, Queen's University, Kingston, Ontario, Canada

Correspondence: Sheela A. Abraham (sa183@queensu.ca)

Received: 28 March 2025 | **Revised:** 25 August 2025 | **Accepted:** 30 September 2025

ABSTRACT

Stem cell niches are complex multi-signalling networks comprised of molecular cues and physical interactions, orchestrated by niche-resident cells and the extracellular factors they produce. The bone niche specifically houses haematopoietic stem cells (HSCs), a critical cell type responsible for producing all blood and immune cells throughout life. Currently, how niches facilitate an ideal environment with simultaneously coordinating both intrinsic and extrinsic cellular signals is unknown. Studies presented here identify the existence of unique extracellular vesicle (EV)-defined niches within the haematopoietic system of human individuals. Bridging studies using proteomic signatures, nanoparticle characterization at single-vesicle resolution and machine learning-based techniques reveal that EVs can be grouped by blood, bone marrow and trabeculae within a human individual. Stem cell assays demonstrate that these niche-defined EVs impart functional effects on stem cells/progenitors based on location within the haematopoietic system. Finally, using single-cell transcriptomic analyses, results identify for the first time how niche-sourced EVs differentially affect the most primitive human HSCs and progenitors. This study highlights the significance of nanoparticles on human immunity and blood production and provides evidence for a new role for EVs, namely the demarcation of distinct nano-niches within biological systems.

Isabelle J. Grenier-Pleau and Christopher J. Wells contributed equally to this work.

1 | Introduction

The haematopoietic system consists of highly specialized cell populations that function in blood clotting, oxygen transport and immune defence (McCulloch et al. 1974). This system is hierarchically organized with rare haematopoietic stem cells (HSCs) positioned at the apex, which give rise to all haematopoietic stem and progenitor cells (HSPCs) that finally culminate into end-state cells (Sawai et al. 2016). Haematopoietic stem cells possess the unique ability to self-renew, differentiate, migrate and enter quiescence in order to be able to maintain all blood and immune cells throughout life (Verovskaya et al. 2019). Mechanisms behind these key functions must be exquisitely controlled to continuously produce 10^{11}–10^{12} mature cells per day (Boulais and Frenette 2015). Although steady-state haematopoiesis is mostly maintained by restricted progenitors (Pietras et al. 2015), primitive HSCs must be preserved indefinitely to maintain physiological blood levels and replenish cell levels during times of depletion, stress and/or infection (Wei and Frenette 2018). The key to long-term conservation of HSCs in adults resides in the microenvironment provided by the bone (Mendelson and Frenette 2014).

Stem cell niches typically provide specialized environments conducive to stem cell homeostasis and are defined by the cells comprising the niche and the soluble factors produced by these resident cells (Ding et al. 2012). To date, murine and zebrafish studies have provided the foundation of understanding regarding HSC niches (Morrison and Scadden 2014; Wattrus and Zon 2018), with the assumption that similar niches exist in humans. However, the regulation of human HSCs, niche function and location remains incompletely understood and rarely explored due to the difficulty of accessing human bone.

The majority of HSCs reside in the bone, which generally consists of a dense exterior (cortical bone) and an inner core. Trabecular bone, a sponge-like porous bone with high turnover, is mainly found at the epiphyseal and metaphyseal regions. These regions flank the diaphysis that contains the bone marrow (Crane et al. 2017; Ellis et al. 2011). Bones are highly vascularized, receiving around 10%–15% of the resting cardiac output, whereas bone vasculature influences the formation and maintenance of niches essential for HSPCs, thus allowing for productive blood cell production (Watson and Adams 2018). Nutrients, oxygen and other factors from the circulation enter the bone marrow mainly through the central artery, which branches into arterioles and then through transitional vessels into a vast network of sinusoids and fenestrated vessels where the exchange of cells and biomolecules takes place. Sinusoids converge into the central sinus, allowing for the exit of HSPCs and waste products from the bone marrow through the venous circulation (Crane et al. 2017; Pinho and Frenette 2019). Despite blood circulation being continuous with the bone and bone marrow, there is a paucity of studies investigating extracellular vesicles (EVs) occupying the bone niche.

Extracellular vesicles are nano-sized (30 nm–10 microns) (Jeppesen et al. 2023) phospholipid particles that are released by cells in an evolutionarily conserved manner, ranging from organisms such as prokaryotes to higher eukaryotes and plants (Lawson et al. 2017; van Niel et al. 2018; Kalluri and LeBleu 2020). Extracellular vesicles contain bioactive cargo such as proteins, nucleic acids, lipids, carbohydrates and metabolites and are able to facilitate molecular signals between cells by virtue of being released by donor cells and subsequently taken up by recipient cells (that can include self) (Colombo et al. 2014). The biological significance of EVs lies in their capacity to transfer information to cells, thereby influencing recipient cell function.

With respect to function, EVs have been implicated in the regulation of coagulation (Noubouossie and Key 2023), angiogenesis (Todorova et al. 2017), reproduction (Simon et al. 2018), embryonic development (Das and Kale 2020), bone calcification (Fang et al. 2024) and HSPC regulation (Butler et al. 2018; Grenier-Pleau and Abraham 2021). In addition, EVs play roles in pathogenesis by stimulating tumor growth (Njock et al. 2022), metabolic reprogramming (Shu et al. 2018; Wang et al. 2023) and evading the immune system (Chen et al. 2018). One of the best-described attributes of tumor-derived EVs is the ability to induce the formation of a pre-/self-reinforcing malignant niche favouring tumor growth (Hoshino et al. 2015; Paggetti et al. 2015). Currently, there are no studies characterizing physiological EV-based niches that exist within human systems during normal homeostatic conditions.

Our group was the first to identify that human blood EV levels are continuously maintained over adulthood and that EVs affect $CD34^+$ cells in an age-dependent manner (Grenier-Pleau et al. 2020). These results prompted us to further our investigations into how EVs from bone niches may influence primitive HSC and specific progenitor cell types. Exclusively using primary human HSPCs and EVs directly enriched from biological fluids, our findings support an unexplored function of EVs—namely compositionally defining niches that exist in blood, bone marrow and trabeculae within humans. Extracellular vesicles within these niches contain unique bioactive constituents and serve to assist with HSC function based on the location within the haematopoietic system. Importantly, we find that niche-based EVs have both common and unique effects on different HSPCs and alter signalling pathways ranging from biogenesis to cell cycle progression based on EV niche and cell type. Our work highlights how nano-scaled biological organization impacts HSC maintenance and contributes to blood and immune cell function.

2 | Methods

2.1 | Ethics

Human sample collection followed the Declaration of Helsinki and was approved by the Queen's University Health Sciences and Affiliated Teaching Hospitals Research Ethics Board (HSREB). Approval for the collection of human umbilical cord blood was obtained prior to commencement of the study (Department Code: DBMS-093-18, TRAQ# 6024642). Informed verbal consent was obtained from all blood donors undergoing total hip arthroplasty surgery according to HSREB regulations.

2.2 | Human Samples

Patient samples (blood [~10 mL/sample], bone marrow [5–15 mL/sample] and trabecular bone [~95 g/sample]) were obtained from consenting participants undergoing total hip arthroplasty surgery at Kingston General Hospital and Hotel Dieu Hospital in Kingston, ON, Canada. Patients were typically diagnosed with osteoarthritis undergoing elective hip replacement. Exclusion criteria included inflammatory arthropathies, cancer, rheumatoid arthritis, any blood disorders and severe systemic cardiovascular or respiratory disease, which would preclude elective surgery. Upon collection, samples were processed immediately and enriched for EVs using protocols described below. Plasma was processed as per (Fuss et al. 2009), unless indicated below, and bone marrow and trabeculae samples were processed as indicated below. More details can be found in (Wells et al. 2025).

HSPCs were obtained from umbilical cord blood (UCB) collected during full-term planned caesarean section surgeries at Kingston General Hospital, Canada. Upon collection, UCB was diluted to a final concentration of 25% in citrate dextrose anticoagulant, then further diluted 1:1 with phosphate-buffered saline (PBS) before layering 30 mL of sample onto 20 mL of Ficoll-Paque Premium (Sigma-Aldrich). Samples were centrifuged at 300 × *g* for 30 min at 21°C to isolate mononuclear cells (MNCs). Each UCB sample was analyzed separately and not pooled. $CD34^+$ cells were obtained from MNCs using CD34 MicroBeads and a QuadroMACS separator (Miltenyi Biotech). HSPCs were either used fresh the same day or frozen at −80°C for later use.

2.3 | PBMC Clonal Haematopoiesis Determination

Peripheral blood mononuclear cells (PBMCs) were isolated and sequenced using a 48-gene panel targeting a pan-myeloid gene list using Ion Torrent next-generation sequencing as previously described (Cook et al. 2019). Variants were excluded if they did not meet criteria for identification (variant allele frequency ≥ 0.02). Subject samples used in this paper were confirmed to have no detectable clonal haematopoiesis of indeterminate potential (CHIP) mutations within the PBMCs.

2.4 | Estimated Trabeculae Volume Calculation

Trabeculae bone weight was determined on the day of surgery, with subsequent drying of the bone for 7–10 days. Mass calculation of 'dry bone' was performed, followed by a rehydration of the dry trabecular bone by total submersion in ddH_2O for 24 h, at which point the rehydrated bone was weighed for a final time. Calculation of available space within the trabecular bone structure was performed as follows:

$$\text{Fraction Available Trabecular Bone Space} = 1 - \left(\frac{\text{Dry Bone g}}{\text{Rehydated Wet Bone g}}\right)$$

The average mass of trabeculae bone pieces collected was 95 g. All 'Fraction Available Trabecular Bone Space' calculations were averaged for males and females, separately, generating a sex-specific 'Fraction Available Trabecular Bone Space' value that was used in all trabecular bone space volume (mL) calculations.

To calculate the volume of space available within the trabecular head that was used to recover EVs, the following calculation was performed:

$$\begin{aligned}&\text{Estimated Trabecular Bone Space (mL)}\\&= (\text{Original Bone Weight}) \times (\text{Fraction Available Space})\\&\times (\text{ddH2O unit Conversion})\end{aligned}$$

where the fraction of available trabecular bone space for females = 0.258, and for males = 0.203. The ddH_2O unit conversion is a constant at 1.002 mL/g. Example: for a female with a trabecular weight of 71 g, the estimated trabecular bone space calculation would be: (71 g) × (0.258) × (1.002 mL/g) = 18.35 mL.

2.5 | Enrichment of EVs

Samples were isolated from the three different haematopoietic regions. The plasma was separated from whole blood after being centrifuged at 1900 × *g* for 10 min at 21°C, followed by a second centrifugation step at 2500 × *g* for 10 min. Bone marrow samples were washed in PBS to remove excess fat and centrifuged at 300 × *g* for 10 min at 21°C. The cell-free bone-marrow-derived supernatant was collected and washed again prior to EV enrichment. Trabecular bone was probed and flushed with PBS before rocking for 10 min at 4°C. The sample was strained through a 40 μm cell strainer and centrifuged at 200 × *g* for 10 min at 21°C. The fat layer was removed, and cell-free supernatant was collected and centrifuged at 300 × *g* for 10 min at 21°C to remove contaminants before EV enrichment.

Samples were enriched for EVs using a 2-step enrichment protocol incorporating iodixanol density cushion (IDC) ultracentrifugation followed by size exclusion chromatography (SEC) (Karimi et al. 2018). Samples were centrifuged at 2500 × *g* for 10 min at 21°C and run through a 40 μm cell strainer to remove remaining fat and debris. Bone marrow and trabecular samples were concentrated using Amicon Ultra-15 10 kDa filters (Sigma-Aldrich) to a total volume of 6 mL. Once processed, samples were layered onto a top-down IDC of 50%, 30%, and 10% Optiprep (Cedarlane). IDC samples were centrifuged at 178,000 × *g* for 2 h at 4°C, using an LS-60 M Ultracentrifuge (Beckman Coulter, USA, cat. No. 347240) with an SW41Ti ultracentrifuge rotor. 1.2 mL of high-density layer (visible interface between the 30% and 10% layers) was collected and further processed using SEC columns (CL2B Sepharose [Sigma-Aldrich]). Samples were collected in 20 fractions of 0.5 mL. EV-containing fractions (7–12) were pooled and aliquoted to minimize freeze-thaw cycles and were stored at −80°C. EVs were thawed on ice and used within 6 months of enrichment. Enriched EV samples were characterized using nanoparticle tracking analysis (NTA) and Qubit Protein Assay Kit (Thermo Fisher Scientific) to determine approximate concentration, size, and protein concentration in solution.

2.6 | Super Resolution Microscopy of EVs

EVs were imaged using the ONi human EV profiler kit v2.0 and processed using stochastic optical reconstruction microscopy (STORM) with the ONi super-resolution nanoimager. EVs were immobilized on microfluidic glass slides and washed of free capture antibodies before fixation and staining. Samples were then stained and imaged with a 3-colour tetraspanin antibody panel (CD81-647, CD63-561, CD9-488 nm) using 30%, 40%, and 50% power on 488, 561, and 640 nm lasers, respectively. Single positive EVs expressed one of CD81, CD63 and CD9 markers, double positive expressed two of the three markers, and triple positive expressed all three markers. EVs were classified as positive for a marker when more than 10 individual localizations were detected in the same channel at a radius of 100 nm around the centre of a cluster.

2.7 | HSPC Incubation With EVs

$CD34^+$ HSPCs were incubated in serum-free media (SFM) supplemented with cytokines and growth factors (IL-3 (20 ng/mL), IL-6 (20 ng/mL), G-CSF (20 ng/mL), Flt3 (100 ng/mL) and SCF (100 ng/mL). The SFM was prepared using Iscove's Modified Dulbecco's Medium (Sigma-Aldrich), bovine serum albumin, insulin, transferrin (B.I.T.) serum substitute, β-mercaptoethanol (Thermo Fisher Scientific), low-density lipoprotein (Sigma-Aldrich), L-Glutamine (Thermo Fisher Scientific), and penicillin/streptomycin (Thermo Fisher Scientific). UCB $CD34^+$ HSPCs were plated at 150,000 cells per mL for 48 h in SFM containing EVs at 10 µg/mL of protein or PBS control. For all incubations, cells were incubated at 37°C with 5% CO_2.

2.8 | Flow Cytometric Analyses

Multiparameter flow cytometry was used for immunophenotyping (Chao et al. 2008; Majeti et al. 2007; Manz et al. 2002; Doulatov et al. 2012) and functional analyses. HSPCs were identified through immunophenotyping using monoclonal antibodies (mAbs) to human CD34 (581), CD38 (HIT2), CD90 (5E10), CD45RA (HI100) and CD123 (6H6) from BD Biosciences. Cells were stained in PBS supplemented with 2% foetal bovine serum (FBS) at 4°C for 45 min on ice, followed by two washes. To determine cell cycle status, UCB $CD34^+$ HSPCs were fixed with 1.5% PFA on ice for 30 min, followed by permeabilization with ice-cold 100% acetone for 10 min. Cells were initially stained with Ki-67 at room temperature for 30 min, followed by CD34 at 4°C for 45 min. Cells were then incubated with DAPI on ice for 7 min and washed before assessment of cell cycle phase. Proliferation kinetics were determined by staining with the fluorescent dye carboxyfluorescein succinimidyl ester (CFSE). $CD34^+$ cells were stained with CFSE for 10 min before incubation in SFM as indicated above. Cellular division was analyzed after 5 days. Fluorescent-Minus-One (FMO) controls using primary cells were used for each experiment. All flow cytometric experiments were subsequently analyzed on FlowJo v10.9.0 software. Flow cytometric experiments were performed on a FACSAria III (BD Biosciences), FACSymphony A3 (BD Biosciences), or a CytoFLEX S (Beckman Coulter) and analyzed using FlowJo v10.9.0 software.

2.9 | Colony-Forming Cell (CFC) Assay

$CD34^+$ cells were incubated with 10 µg/mL EVs enriched from plasma, bone marrow, trabeculae or PBS control. After incubation, 1000 cells from each condition were added to 1.2 mL of H4435-enriched Methocult Medium (StemCell Technologies), plated into 35 mm dishes and incubated at 37°C with 5% CO_2 for 10–12 days. Colonies were quantified and qualified based on morphology using a light microscope. Colony types qualified included colony-forming unit granulocyte/erythrocyte/macrophage/megakaryocyte (CFU-GEMM), colony-forming unit—granulocyte/macrophage (CFU-GM), colony-forming unit—granulocyte (CFU-G), colony-forming unit—macrophage (CFU-M), colony-forming unit erythroid (CFU-E) and burst-forming unit—erythroid (BFU-E).

2.10 | SPARTA Measurements and Spectral Analysis

Single Particle Automated Raman Trapping Analysis (SPARTA) measurements were performed in collaboration with SPARTA Biodiscovery Ltd. (London, UK) and performed on the SPARTA Alpha system. The SPARTA system has been previously described (Penders et al. 2021; Penders et al. 2018). In brief, a 200 µL particle suspension was placed on a 19 mm diameter cover glass (VWR) affixed to a microscope slide. A 63x 1.0 NA water immersion lens (W Plan Apochromat, Zeiss) was then immersed in the droplet. Each trapped particle was imaged for 10 s, with a 2-s shutter time and a 1-s acquisition time for threshold decision. Twenty blank DPBS spectra were measured at 10 s, and their average was used for background subtraction when necessary. Between 151 and 379 single-particle Raman spectra were successfully obtained per sample based on 400 acquisition attempts. Raman spectra were pre-processed using custom MATLAB scripts consisting of a spectral response correction based on a 785 nm excitation standard (National Institute of Standards and Technology, US, SRM2241), post-thresholding to remove aggregates or empty traps, and a 95% background subtraction using the blank DPBS signal. Baseline correction was performed using Whittaker baseline subtraction. Smoothing of the spectra was completed using a first-order Savitzky–Golay filter with a frame size of 7. Each particle spectrum was normalized to the area under the curve. Mean spectra and standard deviation were calculated using MATLAB R2022b and plotted using OriginPro 2023. Principal component analysis (PCA) and partial least squares-discriminant analysis (PLSDA) multivariate statistical modelling were performed using the PLS Toolbox 9.2 (Eigenvector Research Inc.).

2.11 | Mass Spectrometry of EV Samples

Liquid chromatography with tandem mass spectrometry (LC-MS/MS) was performed on tryptic-digested EV samples for proteomic analysis. A total of 18 EV samples from patient-matched plasma ($n = 6$), bone marrow ($n = 6$) and trabeculae ($n = 6$) were analyzed. Samples were reconstituted in 50 mM ammonium bicarbonate with 10 mM Tris(2-carboxyethyl) phosphine hydrochloride (Thermo Fisher Scientific, USA) and vortexed for 1 h at 37°C. Chloroacetamide (Sigma-Aldrich) was added for alkylation to a final concentration of 55 mM. Samples were

vortexed for another hour at 37°C. One microgram of trypsin was added, and digestion was performed for 8 h at 37°C. Samples were dried down and solubilized in 5% ACN-4% formic acid (FA). The samples were loaded on a PepMap Neo C18 pre-column (Thermo Fisher Scientific).

Peptides were separated using a 25 cm Aurora UHPLC Column (IonOpticks) (75 µm i.d. by 250 mm) with a 56-min gradient from 10% to 30% ACN-0.2% FA at a flow rate of 300 nL/min. Subsequent separation was performed on a Neo Vanquish UHPLC system coupled to an Orbitrap Ascend Tribrid Mass Spectrometer (Thermo Fisher Scientific, San Jose, CA, USA). Each full MS spectrum was acquired at a resolution of 120,000 with a 50 ms injection time, followed by tandem-MS (MS-MS) spectra acquisition on the most abundant multiply charged precursor ions for 3 s. Tandem-MS experiments were conducted using higher-energy collision dissociation (HCD) at a collision energy of 27%. The AGC was set to 50%, resolution to 22500, and the injection time to 43 ms. The data was processed using PEAKS X Pro (Bioinformatics Solutions, Waterloo, ON, Canada) and the Uniprot human database (20366 entries). Mass tolerances on precursor and fragment ions were 10 ppm and 0.3 Da, respectively. The fixed modification was carbamidomethyl (C). Variable selected posttranslational modifications were oxidation (M), deamidation (NQ), phosphorylation (STY) and along acetylation (N-ter).

2.12 | Pre-Processing of Proteomic Data

All pre-processing was performed in MATLAB (Mathworks, Inc., MA, USA, version R2023a), as previously (Gerolami et al. 2022). Briefly, 65 duplicate proteins were merged from the original list of 3784, resulting in 3719 unique proteins. Log_2 transformation and imputation of missing values were completed using the 'replaceZeros' function to convert zero values into a value that is 10 in the power of the smallest value of data, followed by data filtration to remove lowly expressed peptides (threshold = 0.4), resulting in a final list of $n = 3433$ proteins. No sample outliers or sequencing batch effects were detected, as confirmed by visual inspection and correlation analysis, as described previously (Panarelli et al. 2019).

2.13 | Feature Selection of Proteomic Data

Mass spectral data were pre-processed, filtered, and analyzed using MATLAB software (v R2023a). Duplicated features were merged, resulting in a dataset of 3433 proteins. Preliminary unsupervised machine learning techniques were performed on all proteins to assess the ability to discriminate the proteomic signatures of EVs by region and by patient. Analysis was visualized using heatmaps and dendrograms as well as Venn diagrams. Proteomic signatures were analyzed for top candidates for discrimination between haematopoietic regions by analysis using a robust feature selection algorithm known as the Molecular Feature Selection Tool (MFeaST) (Gerolami et al. 2022). The most discriminating features were visualized using principal component analysis (PCA) and t-distributed Stochastic Neighbour Embedding (t-SNE) in MATLAB to show clustering (based on similarity) is common by EV source. The top protein candidates for plasma, marrow, and trabeculae were analyzed using hierarchical clustering and visualized in heatmaps and dendrograms using MATLAB.

2.14 | Proteomic Pathway Analysis

To identify enriched pathways in each EV source, the g:Profiler software (Reimand et al. 2007) was used on the protein list ranked by expression ($n = 3433$ proteins) (Abdelhamed et al. 2019). Gene sets corresponding to cellular components of Gene Ontology (GO) (Ashburner et al. 2000), with gene sets being limited to 3 to 500 genes. Statistically significant pathways were selected after multiple testing corrections (Benjamini–Hochberg FDR < 0.05). The Cytoscape Enrichment map built using a standard protocol (Reimand et al. 2019) was used to visualize and interpret statistically enriched cellular components from the three different EV sources (plasma, marrow, trabeculae).

2.15 | Single-Cell Sequencing Analysis

$CD34^+$ UBCs were incubated for 48 h with patient-matched EV samples from plasma ($n = 3$), marrow ($n = 3$), trabeculae ($n = 3$) and PBS control ($n = 3$) (total of 12 samples). After incubation, samples underwent generation of a single-cell library construction using the Chromium Next GEM Single Cell 3' Reagents Kits v3.1 (10X Genomics) with feature barcode technology for cell multiplexing in the protocols outlined by 10X Genomics. Samples were labelled with cell multiplexing oligos prior to pooling. Following multiplexing, samples underwent gel beads-in-emulsion (GEM) generation through the Chromium Controller before cleanup and library construction. Generated libraries were sequenced at 20,000 read pairs per cell for gene expression (GEX) libraries and 5000 read pairs per cell for multiplexing libraries. Libraries were sequenced on an Illumina NovaSeq6000 S4 v1.5, PE100. After sequencing and processing, pooled samples were bioinformatically demultiplexed and analyzed as individual samples.

2.16 | Processing of Single-Cell RNA-Sequencing

Sequenced samples were processed to generate expression matrices. FASTQ files were aligned to the GRCh38 20220-A reference using Cell Ranger count (10x Genomics) (v7.1.0) and filtered, followed by barcode and UMI counting to generate the counts table. RStudio (v4.3.2) and Seurat (v5.0) were used for filtering, variable gene selection, dimensionality reduction and clustering. Filtering removed cells that had unique feature counts over 7000 or less than 200 and had > 8% mitochondrial counts. All genes that were not detected in at least 3 cells were excluded. Datasets were merged and integrated using CCAIntegration. Doublets were removed using DoubletFinder using default settings. Clusters were identified by a graph-based clustering approach implemented by the 'FindCluster' function. Cells embedded in a k-nearest neighbours graph based on a Euclidean distance matrix constructed on significant PCAs (dims = 15, resolutions = 0.8). Cluster 0 represented a heterogeneous cluster; thus, we subclustered it and performed re-clustering (dims = 15, resolution = 0.2) to identify HSCs. New cell IDs were applied to the annotated UMAP. Cell-type-specific markers were determined

using a logFC threshold > 0.6 and an expression in a minimum of 15% of cells. Marker genes that were upregulated in one cluster compared to all other clusters were identified with the 'FindMarkers' function. Clusters were annotated using known HSC and lineage-specific markers. The top seven genes from each cell type cluster were visualized for effective clustering by cell type.

3 | Results

3.1 | Extracellular Vesicles Differ Within the Haematopoietic System of Humans

The vast majority of studies involving haematopoietic EVs are based on blood. During our own investigations into human blood EVs and their effects on $CD34^+$ cells (HSPCs), we hypothesized that the bone milieu might contain niche-specific EVs that differ from those in peripheral blood. To probe this question, EVs were enriched from blood, bone marrow and trabeculae from individual subjects (trio-matched samples) undergoing hip replacement surgeries to directly compare EVs from three different regions of the haematopoietic system (Figure 1a).

To enrich for EVs from blood, bone marrow and trabeculae, our group has developed EV methodology based on guidelines from the International Society of Extracellular Vesicles (ISEV) and a plasma EV enrichment protocol (Welsh et al. 2024; Karimi et al. 2018), as no EV enrichment protocols currently exist for bone marrow and trabeculae samples (see methodology). Our protocol includes a two-step EV enrichment involving an iodixanol density cushion and size exclusion chromatography to obtain EVs devoid of free proteins, DNA, lipoproteins and adipose tissue. When quantifying vesicle size of EVs using nanoparticle tracking analyses, size differences were observed between EVs sourced from various haematopoietic locations, with both bone marrow (139.8 ± 1.8 nm) and trabeculae (144.9 ± 2.0 nm) EVs being larger than plasma (131.4 ± 3.5 nm) EVs (Figure 1b). This result was surprising, as our previous work failed to detect any size differences between blood EVs from individuals aged 20–85 years (Grenier-Pleau et al. 2020) or between healthy and leukaemic blood EVs (unpublished data) using identical methodology. Bone marrow and trabecular regions also possessed significantly higher concentrations of EVs compared to plasma EVs, namely 14-fold ($p < 0.0001$) and 6-fold ($p = 0.0002$) higher, respectively, (Figure 1c) per mL of biological fluid. In contrast, the estimated bulk protein concentration per particle was much lower in both bone-sourced EVs compared to plasma (plasma $1.966 \times 10^{-8} \pm 1.75 \times 10^{-9}$ µg vs. bone marrow $2.277 \times 10^{-9} \pm 3.25 \times 10^{-10}$ µg and trabeculae $1.857 \times 10^{-9} \pm 1.27 \times 10^{-10}$ µg) (Figure 1d). When separating samples by sex, similar results were observed, suggesting that EV size, particle concentration and protein concentration differences between haematopoietic locations are independent of sex (Figure 1e–g). When staining EVs from the various haematopoietic locations with CD9, 63 and 81, the three most common EV tetraspanins, microscopy images were able to confirm all EVs were positive for the three markers (Figure 1h). Interestingly, EVs from the haematopoietic locations differed with respect to the proportions of markers, with bone marrow and trabecular EVs having a higher number of EVs being positive for all three tetraspanins (Figure 1i).

To probe deeper into the differences between haematopoietic niche EVs, unbiased quantitative proteomic studies were performed on trypsin-digested EV proteins from six individuals separated by niche ($n = 18$ total) (Figure 2a). Label-free proteomic profiling of EVs was performed using tandem MS, and a total of 3433 proteins were identified (Table S1). Both the averaged (Figure 2b) and individual (Figure 2c) median protein expression defined niche-specific and overlapping profiles, with similar protein ratios, demonstrating EV protein consistency across 6 individuals.

Machine-learning techniques were used to identify and rank proteins on their ability to discriminate between groups, implementing an established molecular feature selection algorithm (MFeaST) with a leave-one-out validation (Gerolami et al. 2022). This algorithm ranks proteins based on their ability to discriminate between groups, which we have previously shown efficiently identifies features of interest in omics datasets (Grenier-Pleau et al. 2020, Kaczmarek et al. 2022, Panarelli et al. 2019). Using the top-ranking 1% of proteins demonstrates that plasma, bone marrow and trabecular EV proteins have distinguishably defined protein signatures (Figure 2d) (list of ranked proteins in Tables S2–S7). In addition, unsupervised hierarchical clustering analyses successfully and independently delineated groups by sample, as indicated by hierarchical clustering heatmaps and t-distributed stochastic neighbour embedding (t-SNE) plots (Figure 2e), identifying a clear partition between EV proteins from plasma, bone marrow and trabeculae samples.

To annotate subcellular sources of the plasma, bone marrow and trabecular EV proteins, we performed an enrichment analysis (Reimand et al. 2019) using cellular components of Gene Ontology to phenotype vesicle cargo (Figure 2f and Figure S1). The enrichment map suggests that all EVs include proteins associated with the secretory lumen and pigment granules. Bone-sourced EV proteins were specifically associated with energy and ribosomal functions, whereas plasma EV proteins were predominantly associated with immunoglobulins and lipoproteins. Collectively, these data provide evidence that EVs from different regions of the haematopoietic system differ by size and concentration and possess unique protein signatures that originate from particular subcellular compartments.

3.2 | Single Vesicle Resolution Studies Reveal the Discovery of Nanovesicle-Based Niches Within Humans

Raman spectroscopy, a well-established characterization technique, is able to provide label-free compositional data. As a result, Raman spectra yields a molecular fingerprint of the chemical constituents of a sample. To analyse EVs at a single vesicle resolution, Single Particle Automated Raman Trapping Analysis—SPARTA was used. This technique combines Raman spectroscopy with optical trapping, thereby permitting the interrogation of individual EV particles without confounding contributions of substrates. Measurements obtained using this technique permit the analysis of nanoparticles in their native state, providing information about their composition on a single-particle basis. Raman spectra characteristic of EVs were obtained (Figure 3a–c), showing a compositional fingerprint containing strong bands

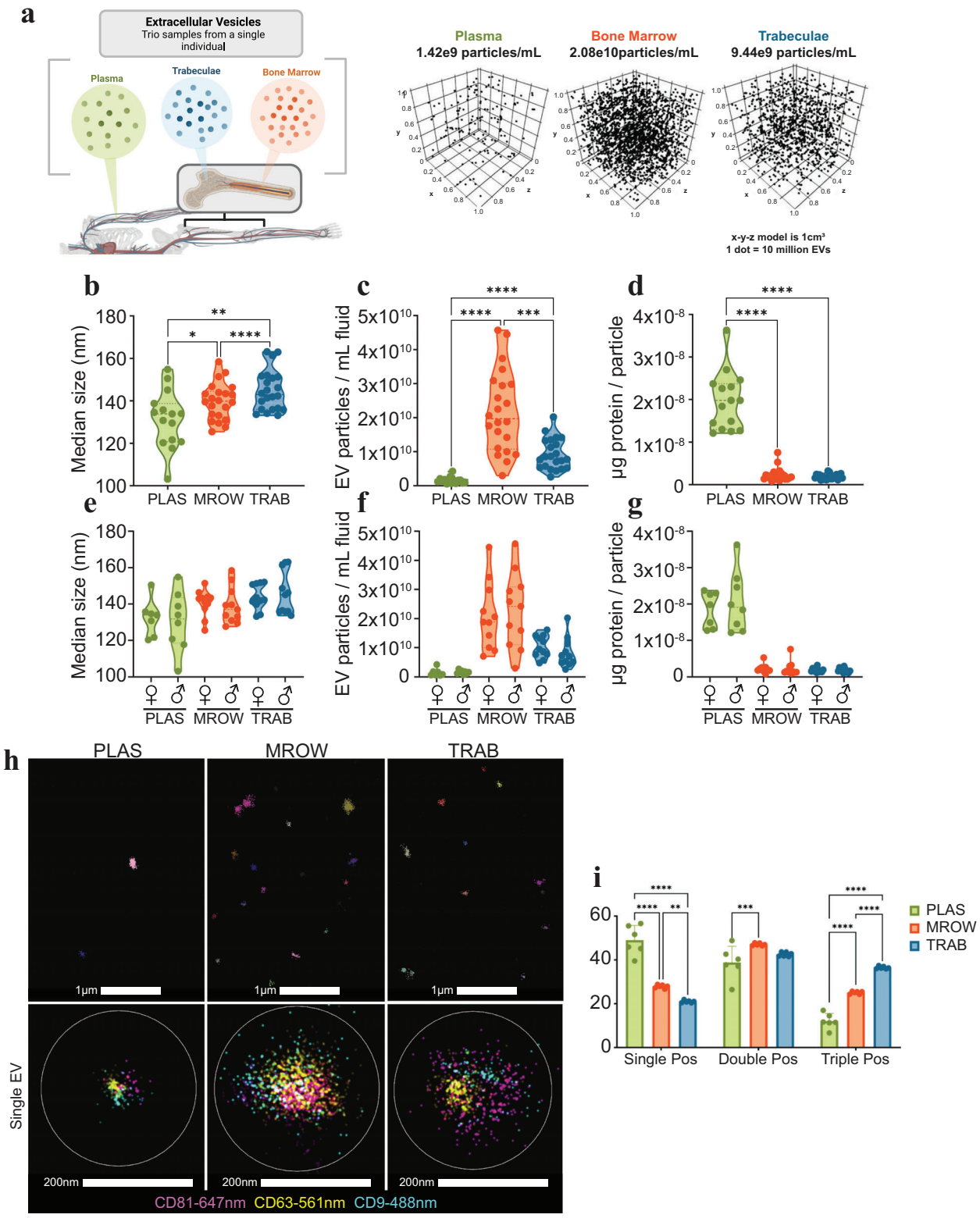

FIGURE 1 | Plasma, bone marrow, and trabecular EVs differ in size, concentration and protein composition. (a) Analysis of EVs from three different haematopoietic regions isolated from single individuals. (b) EV median diameter (nm) (PLAS $n = 15$, MROW/TRAB $n = 22$). (c) EV concentration per mL of sample fluid (PLAS $n = 15$, MROW/TRAB $n = 22$). (d) protein per particle (PLAS $n = 15$, MROW/TRAB $n = 22$) (e–g) Graphs (b-d) separated by sex. In panels (b-d), a mixed-effects statistical analysis with Geisser–Greenhouse correction and Tukey's multiple comparisons test with individual variances was computed for each comparison. (h) Super resolution microscopy images of EVs from plasma, marrow and trabeculae stained with tetraspanins; CD81 (pink), CD63 (yellow), CD9 (blue). (i) Single, double, and triple positive stained EVs (CD81, CD63, CD9), each dot represents EVs in a captured field of view for a total EVs imaged in PLAS = 326, MROW = 22,231, TRAB = 15,779 ($n = 1$). *$p \leq 0.05$, **$p \leq 0.01$, ***$p \leq 0.001$, ****$p \leq 0.0001$.

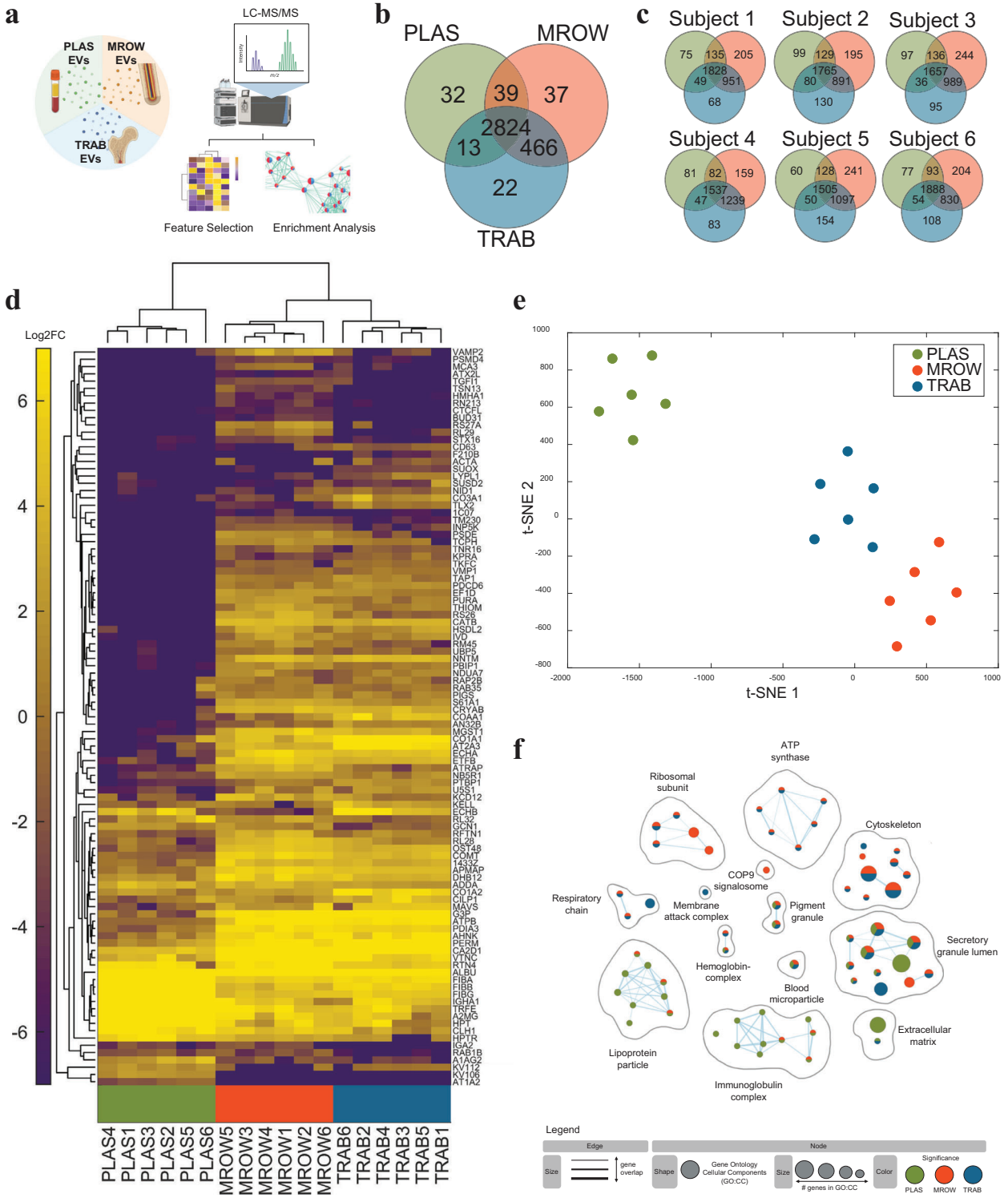

FIGURE 2 | Protein composition differences between plasma, bone marrow and trabecular EVs. (a) Plasma, bone marrow, and trabecular EV protein composition analyzed by LC-MS/MS ($n = 3433$ proteins from 6 subjects totaling 18 samples), visualized by (b) Venn diagram combined or (c) separated by subject. (d) An established feature selection algorithm was used to generate a subset of the top 1% most discriminant proteins between EV source ($n = 101$) visualized as heatmap with dendrogram. (e) t-Distributed stochastic neighbor embedding (t-SNE) plot displays unique protein signatures per EV source. (f) EV proteins analyzed using enrichment analysis of cellular component of Gene Ontology (GO:CC). Statistically significant components were selected after multiple testing correction (Benjamini-Hochberg FDR < 0.05).

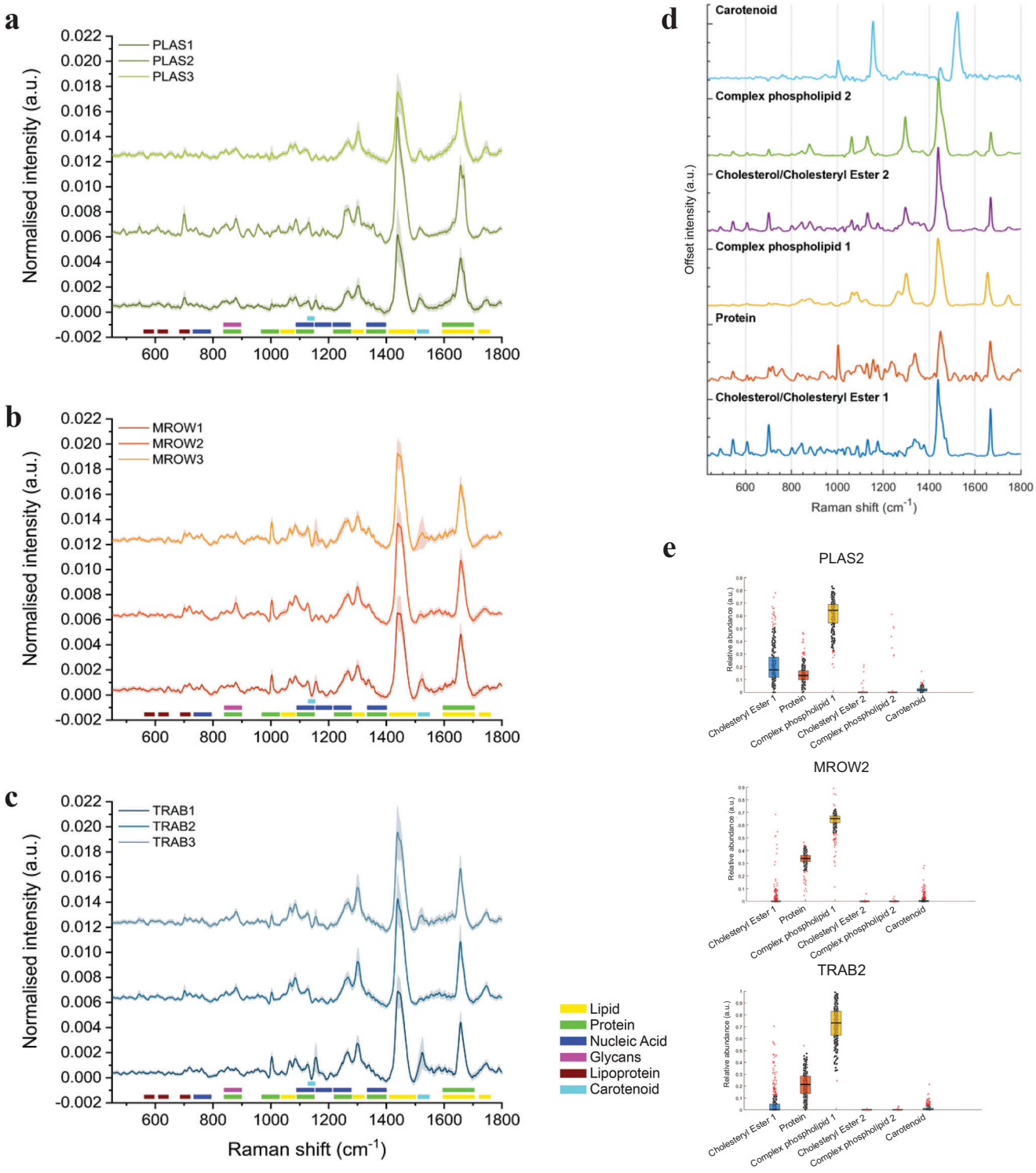

FIGURE 3 | Single particle automated Raman trapping analysis of plasma, bone marrow and trabecular EVs. Raman spectral measurements of single EVs from (a) plasma (PLAS1 $n = 152$), (PLAS2 $n = 296$), (PLAS3 $n = 151$) (b) bone marrow (MROW1 $n = 274$), (MROW2 $n = 198$), (MROW3 $n = 308$). (c) trabecular (TRAB1 $n = 278$), (TRAB2 $n = 379$), (TRAB3 $n = 266$) samples. Spectra shown as mean ± s.d. and coloured bands below the spectra indicate spectral bands assigned to core compositional make up of EVs. (d) Extracted factors using band-target entropy minimization, to recover spectral contributions from biomolecular species that gives rise to the observed, mixed Raman spectra. The extracted factors included carotenoid, complex phospholipid phosphatidylcholine and sphingomyelin, respectively protein and two cholesterol/cholesteryl ester species. (e) Relative abundances of the six extracted factors representative of subject 2 EV isolates (PLAS2, MROW2 and TRAB2). Solid bar marks the median, and red crosses marks outliers below Q1-1.5 IQR and above Q3+1.5 IQR.

TABLE 1 | Extracellular vesicle composition Raman peak assignment.

Band	Vibration/Compound	Raman shift (cm^{-1})
Lipoprotein	Cholesterol	609
Lipoprotein	Cholesterol	698
Nucleic Acids	DNA ring breathing modes	723
Proteins/Glycans	Tyrosine, Glycans	845
Proteins/Glycans	Tryptophan, Glycans	884
Proteins	C-C stretch protein β-sheet	989
Proteins	Phenylalanine	1004
Lipids	C-C stretch lipids	1064
Proteins/Nucleic acids	C-N stretch proteins, PO2 stretch DNA backbone	1084
Carotenoids	υ(C-C) stretch carotene	1155
Proteins/Nucleic acids	C-N stretch proteins	1128
Nucleic acids	Cytosine, Guanine	1185
Proteins/Nucleic acids	Amide-III proteins, DNA ring breathing modes	1256
Lipids	CH2 twist lipids	1295
Proteins/Nucleic acids	Amide-III proteins, DNA ring breathing modes	1337
Proteins/Nucleic acids	Guanine, Tryptophan	1354
Proteins/Nucleic acids	DNA ring breathing modes	1371
Lipids	C=O stretch, CH2 lipids	1399
Lipids	Sphingomyelin	1437
Lipids	CH2 bend lipids	1442
Carotenoids	-C=C- stretch carotene	1520
Proteins	Tryptophan	1622
Proteins/Lipids	Amide-I bonds (C=O), C=C lipid stretch	1655
Lipids	Cholesterol ester	1669
Lipids	C=O stretch lipids	1745

at 1450 cm^{-1} (lipids) for all samples in addition to core bands at 700 cm^{-1} (cholesterol), 1002 cm^{-1} (phenylalanine) and 1100, 1600–1700 cm^{-1} (protein) (see Table 1 for full description of lipoprotein, nucleic acid, proteins, glycans and lipid peak assignments). Observed averaged spectra reveal compositional heterogeneity between plasma (Figure 3a), bone marrow (Figure 3b) and trabeculae (Figure 3c) EVs.

Using entropy minimization, relative abundances of particular species were calculated by unmixing the contributions for each trapped EV, obtaining a compositional distribution for each EV (Figure 3d,e). Through band assignment, protein species, two factors indicating cholesterol/cholesteryl ester (similar to cholesterol and cholesteryl palmitate), two factors indicating complex phospholipids (similar to sphingomyelin and phosphatidylcholine species) and one factor indicating carotenoids were identified. Extracellular vesicles from the three regions displayed different compositional distributions. Carotenoids, a class of isoprenoids predominantly synthesized in plants, were detected in all samples. Dietary-sourced carotenoids can be detected in the blood and bone (Ermakov et al. 2013; Parker 1989), and we hypothesize that, due to their hydrophobic nature, carotenoids can be sequestered into EVs as they are absorbed by lipoproteins (Traber et al. 1994).

To further explore the spectral heterogeneity between the different sourced EV samples, multivariate statistical modelling techniques were implemented. Spectra (Figure 3a–c) were used to construct an unsupervised model, identifying the core variations in the signal in the form of principal component (PC) vectors and giving each spectrum (thus every particle) a score based on similarity to those vectors. Integration of Raman spectra reveal clear clustering based on EV source, which remains consistent across 3 different individuals (Figure 4a–c). Closer inspection of PC2 distinguishes plasma EVs (high positive score on PC2) from bone marrow and trabecular EVs (both negative scores)

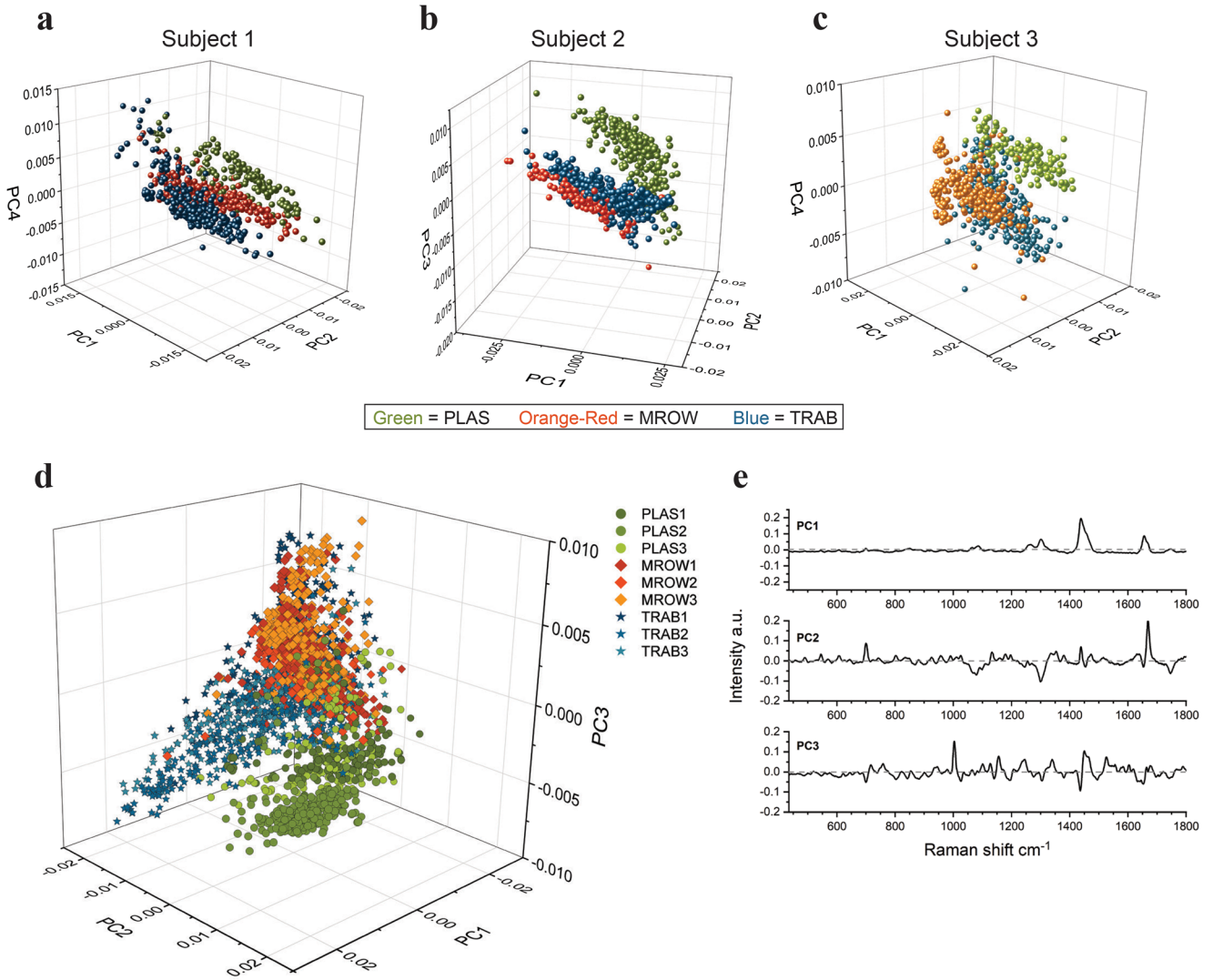

FIGURE 4 | Unsupervised principal component analysis of plasma, bone marrow and trabecular EVs. Raman spectral measurements of single EVs from plasma, bone marrow, and trabecular samples. (a) Unsupervised principal component analyses (PCA) were used to construct models of EV variation between human subjects. Subject-1 EV scores on loading vectors PC1, 2, and 4 for the 5-principal component model. (b) Subject-2 EV scored on loading vectors PC1, 2, and 3 for a 4-principal component model. (c) Subject-3 EV scores on loading vectors PC1, 2, and 4 for a 5-principal component model. Additional subject-specific loading vectors (Extended Figure 2). (d-e) The combination of all Subjects 1-3 EV scores on PC1, 2, and 3 for a 5-principal component model constructed (left) and loading vectors 1, 2, and 3 of the 5-PC model (right).

(Figure S2) and therefore similarly groups them together. Of note, principal component 1 (PC1) largely represents variance in the lipid content of all EVs due to prominent characteristic lipid-associated peaks at 1295, 1442 and 1656 cm^{-1}. PC1 scores largely overlap between plasma, bone marrow and trabeculae, indicating that the lipid content does not distinguish the EV source.

Having explored the intra-sample variations when grouped according to haematopoietic location, PCA modelling was again used to see whether EVs would cluster more closely in terms of haematopoietic location (i.e., plasma, bone marrow, trabeculae) or in terms of human source (i.e., Subjects 1, 2 or 3) (Figure 4d,e). As the model is unsupervised, no information on which spectra belong to which sample class is provided to construct the model. It is clear when constructing a model on the combined (unclassified) data, the spectra clustered into their respective EV niche source (symbol colours of greens, blues and orange-red) rather than according to their subject source (symbol shapes denoted by circles [plasma], diamonds [bone marrow] and stars [trabeculae]).

To provide depth and better separation, a supervised PLSDA model was constructed to specifically quantify the sensitivity and specificity between EVs from each haematopoietic niche. Very clear distinctions can be made between the samples, with minimal overlap in the clusters (Figure S2). This is also confirmed by the very high cross-validated sensitivity (88.5%–97.9%) and specificity (87.3%–98.1%) values obtained, as shown in (Table S1). When viewing these results as a whole, the differing Raman spectra from different haematopoietic niches support our hypothesis that niches within the haematopoietic system possess a unique composition of EVs at a nanoparticle level.

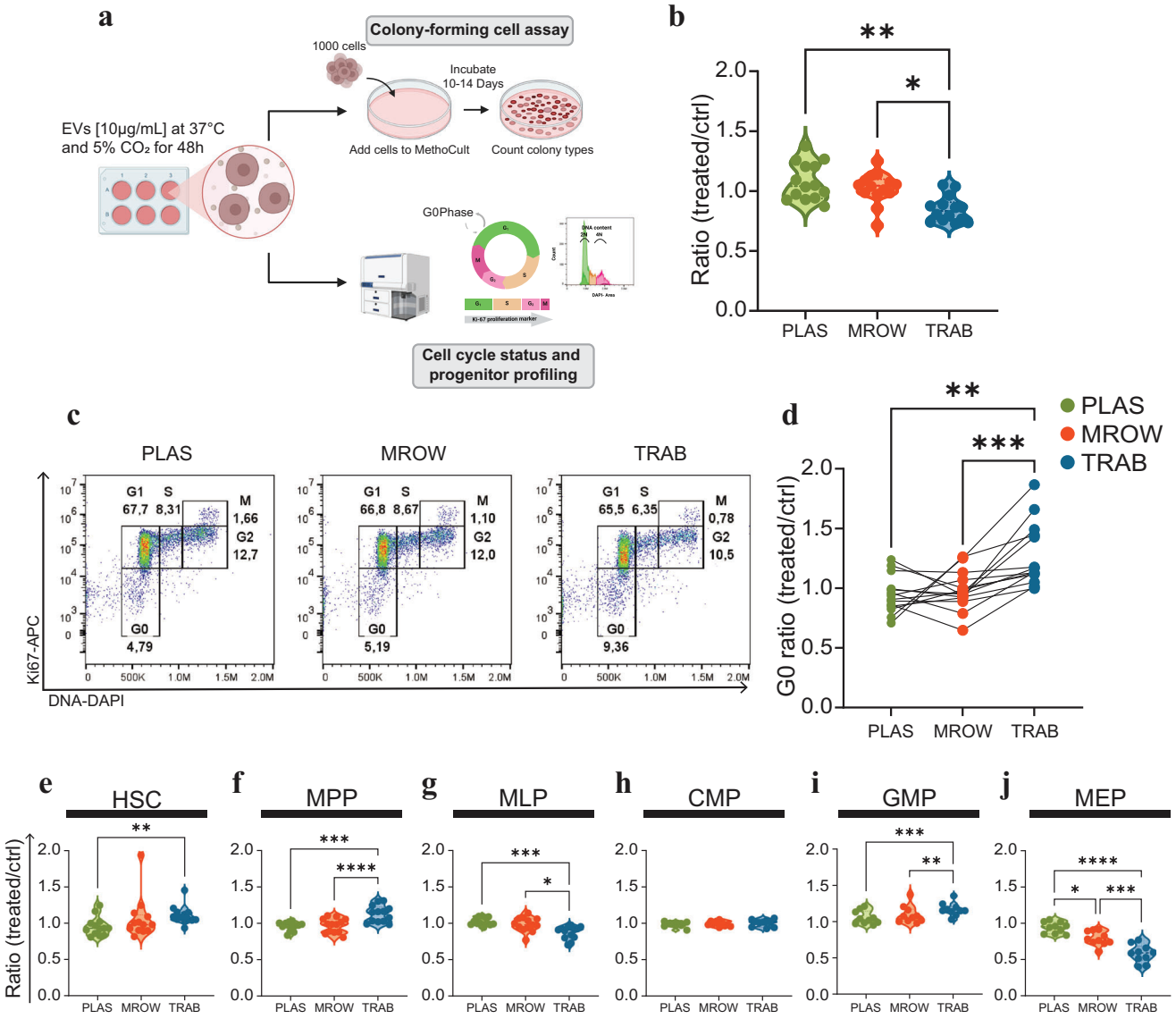

FIGURE 5 | Functional effects of plasma, bone marrow and trabecular EVs on HSPC populations. Umbilical cord blood CD34+ cells were incubated with either plasma, marrow or trabecular sourced EVs for 48 h. (a) Experimental design to assess the functional impact of plasma, bone marrow and trabecular EVs on HSPCs. (b) Ratio of total number of colonies normalized to PBS control (n = 14 plasma; n = 14 marrow; n = 14 trabeculae). (c) Cell cycle analysis of HSPCs after 48 h incubation with the 3 EV niche sources. Representative flow cytometry plot of cell cycle populations (d) Ratio of quiescent G0 phase normalized to PBS control, paired by EV subject as indicated with lines ($n = 14$). (e-j) Flow cytometry HSPC panel after 48 h incubation with 3 EV niche sources, normalized to PBS control. Ratio of (e) HSC, (f) MPP, (g) MLP (n = 13), and (h) CMP, (i) GMP, (j) MEP cells ($n = 10$). Haematopoietic stem cell (HSC); multipotent progenitor (MPP); multipotent lymphoid progenitor (MLP); common myeloid progenitor (CMP); granulocyte-monocyte progenitor (GMP); megakaryocyte-erythroid progenitor (MEP). Statistical analysis: RM one-way ANOVA, with Geisser–Greenhouse correction, along with Tukey's multiple comparisons test with individual variances computed for each comparison *$p \leq 0.05$, **$p \leq 0.01$,***$p \leq 0.001$, ****$p \leq 0.0001$.

3.3 | Niche EVs Have Functional Effects on Haematopoietic Stem Cells and Progenitors

To ascertain if EVs from different haematopoietic niches impart functional effects with respect to proliferation and differentiation capacity, in vitro colony-forming cell (CFC) assays were performed using cord blood-sourced CD34$^+$ (HSPCs) (Figure 5a). Cells were incubated with EVs from the different niches for 48 h, followed by plating cells in methylcellulose media with defined growth factors. Enumerated colony counts indicate that HSPCs incubated with trabeculae-sourced EVs display decreased colony-forming ability compared to plasma and bone marrow-EV-incubated HSPCs (Figure 5b). To ascertain if EVs influenced cell cycle transitions, CD34$^+$ HSPCs were incubated with the indicated EVs for 48 h, which was followed by staining with Ki-67 and DAPI and subsequent flow cytometry analyses. Representative (Figure 5c) and averaged flow cytometry data normalized to PBS control (Figure 5d) suggest that incubation of HSPCs with trabecular EVs almost doubles the number of cells in quiescence compared to both plasma- and bone marrow-sourced EVs (Figure 5c). These results also support the notion that EVs within a single individual within different haematological regions are more different than plasma EVs from different individuals.

Next, it was determined if EVs from different niches have an effect on the stemness of HSPCs. $CD34^+$ HSPCs were incubated in vitro with the indicated EVs for 48 h, followed by staining with fluorescent conjugated antibodies (CD34, CD38, CD45RA, CD90 and CD123) to identify stem and progenitor populations, using flow cytometry (Figure 5e-j with gating strategy indicated in Figure S4). Trabecular-sourced EVs had the most significant effect on specific populations—increasing both HSCs (Figure 5e), multipotent progenitors (MPPs) (Figure 5f) and granulocyte-monocyte progenitors (GMPs) (Figure 5i) but decreasing both multipotent lymphoid progenitors (MLPs) (Figure 5g) and megakaryocyte-erythrocyte progenitors (MEPs) (Figure 5j). It is important to appreciate that the data presented in Figure 5 are subject to two levels of biological variability—the sources of EVs are from different sources, and the HSPCs are collected from different umbilical cord sources. Despite these biological variables, trabecular niche EVs consistently show significant effects on human HSPCs.

3.4 | Nano-Niche EVs Initiate Both Common and Unique Transcriptional Signals Within Haematopoietic Stem Cells and Progenitor Populations at a Single Cell Level

To understand what EV-niche-based effects were being imparted on haematopoietic cells at a transcriptional level, single-cell RNA sequencing was performed on $CD34^+$ cells 48 h post-EV exposure, using the 10X Genomics platform. Cell multiplexing was utilized to obtain transcriptional data from the three different subjects, thus avoiding potential confounding effects from a single individual. A total of 45,750 single-cell transcriptomes were subjected to Louvain clustering, resulting in 12 transcriptionally distinct populations in our combined analysis of 4 EV treatment groups (PLAS, MROW, TRAB, PBS) from 3 individuals per condition (Figure 6a). Haematopoietic stem cells and progenitors were annotated based on differentially expressed gene (DEG) analysis (Figure 6b and Figure S5), thereby allowing the identification of the most primitive HSCs, MPPs and progenitors. All cells corresponding to a specified annotated cell type and treatment group were aggregated together by summation into a single pseudobulk sample. The DESEQ2 pipeline was then used to conduct pairwise comparisons of all genes between each EV treatment group versus PBS control.

To interrogate the top biological processes, signatures, and pathways associated with our dataset, we used Ingenuity Pathway Analysis (IPA). A total of 92 biological functions were identified across all 12 cell types after two-step filtering: (1) multiple testing correction (Benjamini–Hochberg FDR < 0.05) and (2) if at least one condition had an absolute z-score of ≥ 2. Common functions that were upregulated by all EVs included the biosynthesis and breakdown of macromolecules and proteins (Figure 6c). Other than these functions, plasma EVs affected very few cell types exclusively. In contrast, bone marrow and trabecular EVs modulated multiple functions within HSPCs, eliciting both common and unique processes depending on cell type (Figure 6c). When specifically focusing on activated or inhibited biological functions in the non-committed HSPC populations, that is, more primitive cell types (Figure 7a), using stringent thresholds of an absolute z-score of ≥ 2, no biological functions were enriched within HSC or MPP populations when exposed to plasma EVs. These results are in alignment with the fact that HSC and MPP populations would rarely frequent the plasma niche. Contrary to plasma EVs, EVs derived from the bone marrow or trabeculae increased mitochondrial biogenesis, cell survival pathways and clathrin-mediated endocytosis, while downregulating apoptotic signalling. Specifically, within the HSC population, bone marrow EVs transcriptionally enhanced genes involved with the biosynthesis of macromolecules and synthesis of proteins with inhibiting post-translational modifications (e.g., ubiquitin and phosphorylation) and reactive oxygen species (ROS). Trabecular EVs had different effects on HSCs, namely altering genes involved with cell cycle progression, repair of DNA and association with chromatin (all B-H P-values and z-scores for non-committed HSPCs in Table S10). Inhibition of cell cycle progression as a function was not found to be significant in any cell type or EV condition, with the exception of trabecular EV-treated HSCs. Because these results supported observations that trabeculae EVs dampen the colony-forming ability and increase the quiescence of HSPCs (Figure 5b–d), a closer inspection of genes associated with cell cycle progression was completed. Gene expression profiles identified in Figure 7b,c support cell cycle inhibition. The expression of *MKI-67*, *TP53* and *MDM2* expression are additionally congruent with increased quiescence in the HSC population. p53 is a key modulator of quiescence in HSCs (Liu et al. 2009; Asai et al. 2012), and the absence of *MKI-67* is associated with a quiescent state. Taken as a whole, results support the observation that niche-based EVs have different transcriptional effects on different cell types, and trabeculae niche EVs specifically promote quiescence in HSCs (Figure 7d). We posit that long-term HSCs receive important signalling cues from trabeculae niche EVs in order to maintain lifelong haematopoiesis.

4 | Discussion

Results presented here represent the first comprehensive study comparing EVs from three different regions of the human haematopoietic system and identify a new function of EVs—defining homeostatic niches within humans. Currently, the majority of human haematopoietic EV studies are based on blood (Abdelhamed et al. 2019; Doron et al. 2019; Peng et al. 2021), and no studies exist investigating the impact human bone marrow or trabecular EVs have on HSCs, largely due to the difficulty in obtaining healthy bone tissue. To address this, we utilized bone samples from individuals undergoing hip arthroplasty, with the majority of patients having osteoarthritis. These tissues are considered a suitable proxy for healthy bone (Chang et al. 2014). This study is first to provide evidence of EVs altering both functional and transcriptional events within the most primitive HSCs.

Elegant murine studies have succinctly identified specific bone niches defined by location (perisinusoidal) (Kiel et al. 2005) and cell type (e.g., leptin receptor+ mesenchymal stromal and endothelial cells [Ding et al. 2012]). The concept that distinct domains around certain regions in the bone regulate and maintain different kinds of stem cells and progenitors has already been suggested (Comazzetto et al. 2021). Our work supports this idea and is not incongruent with detailed mouse studies investigating HSC localization but may highlight the need to include EV composition within very localized regions of bone

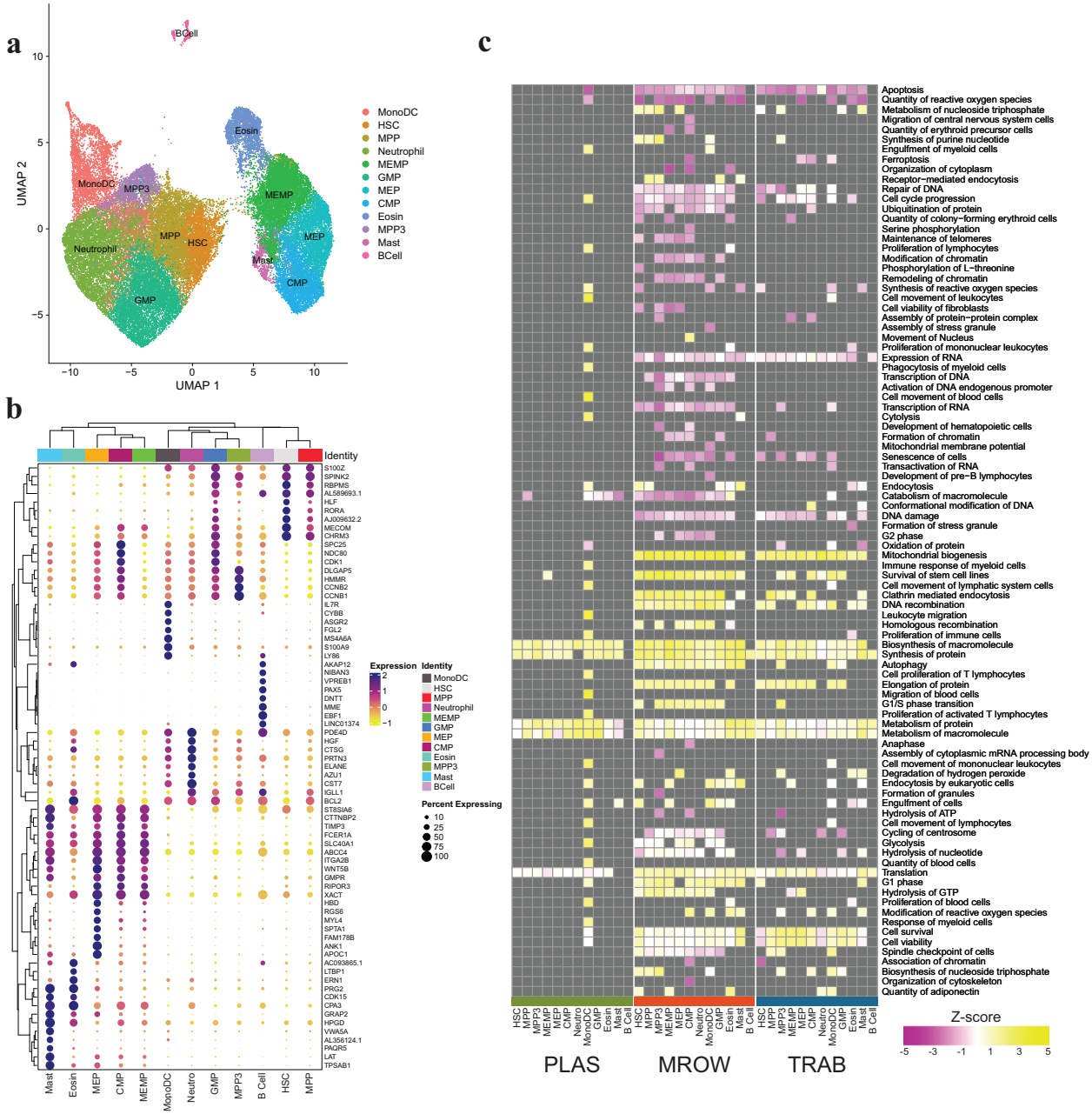

FIGURE 6 | Niche-based EVs initiate both common and unique transcriptional profiles in HSPCs. Single-cell RNA-seq (scRNA-seq) was performed on CD34+ enriched HSPCs post 48 h incubation with plasma, marrow, or trabecular EVs, or PBS control. (a) Cell annotation of 12 haematopoietic cell types using UMAP embedding of the scRNAseq data ($n = 45{,}750$ transcriptomes). (b) Dotplot displays haematopoietic gene set used for cell annotation of cell types in scRNAseq data. (c) Heatmap displays z-score of top 92 biological functions classified by IPA from specific annotated cell types. Only significant biological functions (Benjamini–Hochberg FDR < 0.05) displayed with z-score ranging from -5 to +5. Biological functions not reaching significance are displayed in grey.

marrow and trabeculae. It is important to highlight that the work presented here is solely based on human HSPCs and human EVs directly enriched from the indicated biological fluid. By not using culture-conditioned EVs, studies here represent a step forward in attempts to understand biological niches, despite the existing limitations of studying human systems.

Our results show that only trabecular EVs upregulate p53 in contrast to plasma and bone marrow EVs. Because p53 regulates quiescence in HSCs (Liu et al. 2009), we speculate that trabecular EVs may be important in long-term maintenance of the small population of HSCs that must be maintained throughout life. Investigation of this hypothesis will undoubtedly lead to a better understanding of how the haematopoietic system is able to sustain lifelong blood and immune cell function and how EVs may play a role in this critical function.

Substantive evidence supports the idea that EVs released from cancer cells alter the tumor microenvironment to foster malignant growth (Hoshino et al. 2015; Peinado et al. 2012; Kumar et al.

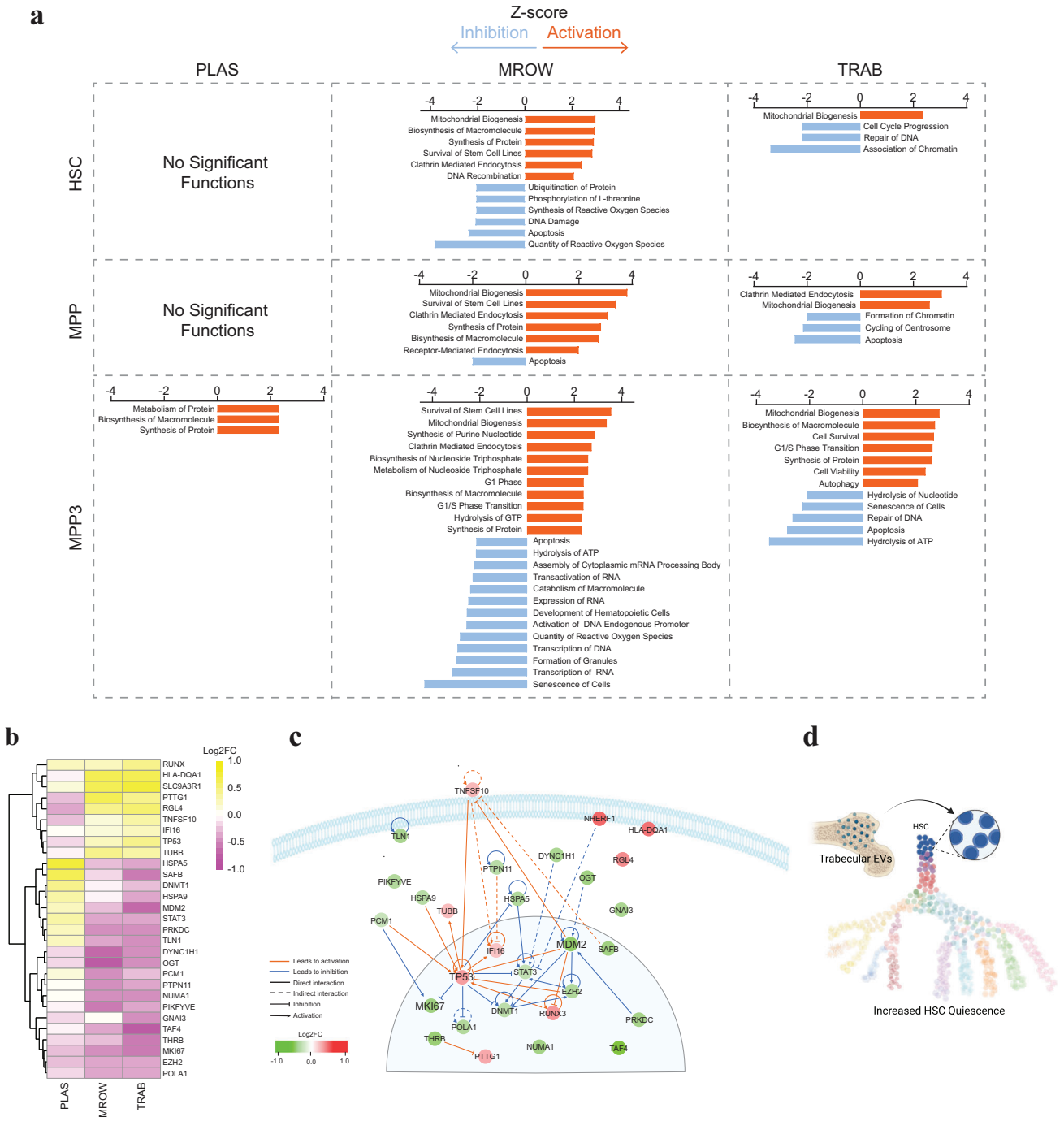

FIGURE 7 | Trabecular EVs downregulate cell cycle progression in the most primitive HSPC populations. Single-cell RNA-seq (scRNA-seq) was performed on CD34+ enriched HSPCs post 48 h incubation with plasma, marrow, or trabecular EVs or PBS control. (a) Bar plot listing biological functions specifically enriched in HSC, MPP, MPP3 populations, significant by both FDR < 0.05 and by *z*-score absolute value of ≥ ±2. (b) Heatmap of log2 fold change differential expression of 29 genes involved in cell cycle progression significantly altered in HSCs upon trabecular EV exposure. (c) Schematic illustrating gene network of the 29 genes presented in (b). (d) Summary graphic of trabecular EVs on HSCs.

2018). Specifically, EVs isolated from acute myeloid leukaemia (AML) patients are able to downregulate the expression of p53 and its cell cycle target gene p21 in bone marrow mesenchymal cells (Ghanam et al. 2023). Our current study suggests that trabecular EVs may play a non-cell autonomous protective role in maintaining sufficiently high levels of p53 in older subjects, which may be potentially altered in the presence of leukaemic EVs, leading to a decrease of p53 expression (Abraham et al. 2016). Future studies will need to confirm if other signalling nodes are affected by EV-maintained microenvironments under physiological or disease conditions.

Our results confirm that EVs from plasma, bone marrow and trabeculae are distinctly different with respect to composition and conferring function, which may potentially impact clinical studies investigating biomarkers and therapeutics involved with

mesenchymal stem cells or bone marrow transplants. We hope our study highlights the effects location-based EVs may have on bone-resident cells.

In summary, this study presents evidence that within the haematopoietic system, there exist different EV niches, defined by EV composition, and that these niches can be reproducibly found in multiple individuals. Importantly, EV niches impart both common and specific functions on different cell types. We posit that the EV niches identified may have critical roles to play in the regulation of other bone-resident cells, such as mesenchymal stem cells, osteocytes, osteoblasts, osteoclasts, endothelial and stromal cells. We speculate that EV niches exist in other human systems in the body, such as the respiratory, urinary and nervous systems; however, this needs to be validated with future studies. We also hypothesize that our findings will shed insight into investigations focused on clonal haematopoiesis, bone cancer and leukaemia.

4.1 | Limitations of Study

Based on our enrichment protocol, our study is limited to small EVs between 30 and 300 nm. We anticipate that, based on the different locations with differing cell composition, other EV subtypes, such as large EVs, would likely differ; however, these results must be confirmed.

This study aims to investigate different haematopoietic locations under physiological conditions. An additional limitation to this investigation is that the majority of the study population had osteoarthritis (De Roover et al. 2023), requiring an elective hip replacement. Although our exclusion criteria included participants with inflammatory arthropathies, cancer, rheumatoid arthritis, any blood disorder, severe systemic cardiovascular or respiratory disease precluding elective surgery, we cannot negate this as an important detail. It is important to note that no significant changes in inflammatory signalling in any cell type or EV-treated condition were detected.

Finally, all HSPC samples were obtained from umbilical cord blood. We chose this stem cell and progenitor source based on the fact that the cells have negligible genetic or epigenetic alterations and thus serve as an 'untouched' and 'un-aged' population of stem cells to analyse EV-mediated alterations. We acknowledge that using young HSPCs versus samples from older individuals may have different results, which should be evaluated in a separate study.

Author Contributions

Isabelle J. Grenier-pleau: methodology, formal analysis, validation, writing - review and editing, investigation, visualization, writing–original draft. **Christopher J. Wells**: methodology, validation, formal analysis, writing–review and editing, investigation, visualization, writing–original draft. **Samantha M. Holmes**: investigation, visualization, writing–review and editing. **Christine Hall**: methodology, investigation. **Michael Vermeulen**: investigation. **Camille A. de Villiers**: investigation. **Jelle Penders**: methodology, investigation. **Simon Vilms Pedersen**: investigation. **Sarah A. Dick**: investigation. **Eric Bonneil**: investigation. **Mykhaylo Slobodyanyuk**: investigation. **Murtaza S. Nagree**: investigation. **Jasleen Kaur**: investigation. **Jamie Beaulieu**: investigation. **Molly M. Stevens**: supervision, writing–review and editing. **Stephanie Z. Xie**: supervision, writing–review and editing. **Michael J. Rauh**: supervision. **Lynne-Marie Postovit**: supervision. **Jüri Reimand**: supervision, writing–review and editing. **Kathrin Tyryshkin**: supervision, writing–review and editing. **Pierre Thibault**: supervision, writing–review and editing. **Andrew Craig**: supervision. **John F. Rudan**: investigation. **Steve Mann**: investigation, writing–review and editing. **Sheela A. Abraham**: conceptualization, visualization, writing–original draft, supervision, resources, funding acquisition, writing–review and editing. **Amy J.M. Mcnaughton**: project administration. **David J.H.F. Knapp**: supervision. **Edmond Y.W. Chan**: supervision, writing–review and editing.

Funding

Canadian Institutes of Health Research grant 394568 (SAA). Canadian Institutes of Health Research grant PGF175484. The Terry Fox New Frontiers Program Project Grant 6039065 (SAA). Terry Fox New Investigator Grant 1133 (SAA).

Conflicts of Interest

Authors declare that they have no competing interests with the following exception. M.M.S. and J.P. are co-founders of Sparta Biodiscovery Ltd. and are inventors in a patent describing the single particle Raman spectroscopy technique SPARTA (1810010.7). C.A.d.V. is a consultant at Sparta Biodiscovery Ltd. M.M.S. invested in, consults for (or was on scientific advisory boards or boards of directors), and conducts sponsored research funded by companies related to the biomaterials field.

Data Availability Statement

All data are available in the main text, extended data or (to be) deposited in an appropriate repository. The data that support the findings of this study are available from the corresponding author upon reasonable request.

References

Abdelhamed, S., J. T. Butler, B. Doron, et al. 2019. "Extracellular Vesicles Impose Quiescence on Residual Hematopoietic Stem Cells in the Leukemic Niche." *EMBO Reports* 20: e47546. https://doi.org/10.15252/embr.201847546.

Abraham, S. A., L. E. M. Hopcroft, E. Carrick, et al. 2016. "Dual Targeting of p53 and c-MYC Selectively Eliminates Leukaemic Stem Cells." *Nature* 534: 341–346. https://doi.org/10.1038/nature18288.

Asai, T., Y. Liu, S. Di Giandomenico, et al. 2012. "Necdin, a p53 Target Gene, Regulates the Quiescence and Response to Genotoxic Stress of Hematopoietic Stem/Progenitor Cells." *Blood* 120: 1601–1612. https://doi.org/10.1182/blood-2011-11-393983.

Ashburner, M., C. A. Ball, J. A. Blake, et al. 2000. "Gene Ontology: Tool for the Unification of Biology. The Gene Ontology Consortium." *Nature Genetics* 25: 25–29. https://doi.org/10.1038/75556.

Boulais, P. E., and P. S. Frenette. 2015. "Making Sense of Hematopoietic Stem Cell Niches." *Blood* 125: 2621–2629. https://doi.org/10.1182/blood-2014-09-570192.

Butler, J. T., S. Abdelhamed, and P. Kurre. 2018. "Extracellular Vesicles in the Hematopoietic Microenvironment." *Haematologica* 103: 382–394. https://doi.org/10.3324/haematol.2017.183335.

Chang, H., D. Docheva, U. R. Knothe, and M. L. Knothe Tate. 2014. "Arthritic Periosteal Tissue From Joint Replacement Surgery: A Novel, Autologous Source of Stem Cells." *Stem Cells Translational Medicine* 3: 308–317. https://doi.org/10.5966/sctm.2013-0056.

Chao, M. P., J. Seita, and I. L. Weissman. 2008. "Establishment of a Normal Hematopoietic and Leukemia Stem Cell Hierarchy." *Cold Spring Harbor*

Symposia on Quantitative Biology 73: 439–449. https://doi.org/10.1101/sqb.2008.73.031.

Chen, G., A. C. Huang, W. Zhang, et al. 2018. "Exosomal PD-L1 Contributes to Immunosuppression and Is Associated With Anti-PD-1 Response." *Nature* 560: 382–386. https://doi.org/10.1038/s41586-018-0392-8.

Colombo, M., G. Raposo, and C. Théry. 2014. "Biogenesis, Secretion, and Intercellular Interactions of Exosomes and Other Extracellular Vesicles." *Annual Review of Cell and Developmental Biology* 30: 255–289. https://doi.org/10.1146/annurev-cellbio-101512-122326.

Comazzetto, S., B. Shen, and S. J. Morrison. 2021. "Niches That Regulate Stem Cells and Hematopoiesis in Adult Bone Marrow." *Developmental Cell* 56: 1848–1860. https://doi.org/10.1016/j.devcel.2021.05.018.

Cook, E. K., T. Izukawa, S. Young, et al. 2019. "Comorbid and Inflammatory Characteristics of Genetic Subtypes of Clonal Hematopoiesis." *Blood Advances* 3: 2482–2486. https://doi.org/10.1182/bloodadvances.2018024729.

Crane, G. M., E. Jeffery, and S. J. Morrison. 2017. "Adult Haematopoietic Stem Cell Niches." *Nature Reviews Immunology* 17: 573–590. https://doi.org/10.1038/nri.2017.53.

Das, M., and V. Kale. 2020. "Extracellular Vesicles: Mediators of Embryo-maternal Crosstalk During Pregnancy and a New Weapon to Fight Against Infertility." *European Journal of Cell Biology* 99: 151125. https://doi.org/10.1016/j.ejcb.2020.151125.

De Roover, A., A. Escribano-Nunez, S. Monteagudo, and R. Lories. 2023. "Fundamentals of Osteoarthritis: Inflammatory Mediators in Osteoarthritis." *Osteoarthritis and Cartilage* 31: 1303–1311. https://doi.org/10.1016/j.joca.2023.06.005.

Ding, L., T. L. Saunders, G. Enikolopov, and S. J. Morrison. 2012. "Endothelial and Perivascular Cells Maintain Haematopoietic Stem Cells." *Nature* 481: 457–462. https://doi.org/10.1038/nature10783.

Doron, B., S. Abdelhamed, J. T. Butler, S. K. Hashmi, T. M. Horton, and P. Kurre. 2019. "Transmissible ER Stress Reconfigures the AML Bone Marrow Compartment." *Leukemia* 33: 918–930. https://doi.org/10.1038/s41375-018-0254-2.

Doulatov, S., F. Notta, E. Laurenti, and J. E. Dick. 2012. "Hematopoiesis: A Human Perspective." *Cell Stem Cell* 10: 120–136. https://doi.org/10.1016/j.stem.2012.01.006.

Ellis, S. L., J. Grassinger, A. Jones, et al. 2011. "The Relationship Between Bone, Hemopoietic Stem Cells, and Vasculature." *Blood* 118: 1516–1524. https://doi.org/10.1182/blood-2010-08-303800.

Ermakov, I. V., M. R. Ermakova, T. D. Rosenberg, and W. Gellermann. 2013. "Optical Detection of Carotenoid Antioxidants in Human Bone and Surrounding Tissue." *Journal of Biomedial Optics* 18: 117006. https://doi.org/10.1117/1.JBO.18.11.117006.

Fang, F., J. Yang, J. Wang, et al. 2024. "The Role and Applications of Extracellular Vesicles in Osteoporosis." *Bone Research* 12: 4. https://doi.org/10.1038/s41413-023-00313-5.

Fuss, I. J., M. E. Kanof, P. D. Smith, and H. Zola. 2009. "Isolation of Whole Mononuclear Cells From Peripheral Blood and Cord Blood." *Current Protocols in Immunology* 7, no. 1: 7.1.1–7.1.8. https://doi.org/10.1002/0471142735.im0701s85.

Gerolami, J., J. J. M. Wong, R. Zhang, et al., 2022. "A Computational Approach to Identification of Candidate Biomarkers in High-Dimensional Molecular Data." *Diagnostics* 12: 1997. https://doi.org/10.3390/diagnostics12081997.

Ghanam, J., V. K. Chetty, S. Anchan, et al. 2023. "Extracellular Vesicles Transfer Chromatin-Like Structures That Induce Non-Mutational Dysfunction of p53 in Bone Marrow Stem Cells." *Cell Discovery* 9: 12. https://doi.org/10.1038/s41421-022-00505-z.

Grenier-Pleau, I., and S. A. Abraham. 2021. "Extracellular Vesicles Tell All: How Vesicle-Mediated Cellular Communication Shapes Hematopoietic Stem Cell Biology With Increasing Age." *Experimental Hematology* 101-102: 7–15. https://doi.org/10.1016/j.exphem.2021.08.004.

Grenier-Pleau, I., K. Tyryshkin, T. D. Le, et al. 2020. "Blood Extracellular Vesicles From Healthy Individuals Regulate Hematopoietic Stem Cells as Humans Age." *Aging Cell* 19: e13245. https://doi.org/10.1111/acel.13245.

Hoshino, A., B. Costa-Silva, T.-L. Shen, et al. 2015. "Tumour Exosome Integrins Determine Organotropic Metastasis." *Nature* 527: 329–335. https://doi.org/10.1038/nature15756.

Jeppesen, D. K., Q. Zhang, J. L. Franklin, and R. J. Coffey. 2023. "Extracellular Vesicles and Nanoparticles: Emerging Complexities." *Trends in Cell Biology* 33: 667–681. https://doi.org/10.1016/j.tcb.2023.01.002.

Kaczmarek, E., B. Pyman, J. Nanayakkara, et al. 2022. "Discriminating Neoplastic From Nonneoplastic Tissues Using an miRNA-Based Deep Cancer Classifier." *American Journal of Pathology* 192: 344–352. https://doi.org/10.1016/j.ajpath.2021.10.012.

Kalluri, R., and V. S. LeBleu. 2020. "The Biology, Function, and Biomedical Applications of Exosomes." *Science* 367: eaau6977. https://doi.org/10.1126/science.aau6977.

Karimi, N., A. Cvjetkovic, S. C. Jang, et al. 2018. "Detailed Analysis of the Plasma Extracellular Vesicle Proteome After Separation From Lipoproteins." *Cellular and Molecular Life Sciences* 75: 2873–2886. https://doi.org/10.1007/s00018-018-2773-4.

Kiel, M. J., Ö. H. Yilmaz, T. Iwashita, O. H. Yilmaz, C. Terhorst, and S. J. Morrison. 2005. "SLAM family Receptors Distinguish Hematopoietic Stem and Progenitor Cells and Reveal Endothelial Niches for Stem Cells." *Cell* 121: 1109–1121. https://doi.org/10.1016/j.cell.2005.05.026.

Krämer, A., J. Green, J. Pollard, and S. Tugendreich. 2014. "Causal Analysis Approaches in Ingenuity Pathway Analysis." *Bioinformatics* 30: 523–530. https://doi.org/10.1093/bioinformatics/btt703.

Kumar, B., M. Garcia, L. Weng, et al. 2018. "Acute Myeloid Leukemia Transforms the Bone Marrow Niche Into a Leukemia-Permissive Microenvironment Through Exosome Secretion." *Leukemia* 32: 575–587. https://doi.org/10.1038/leu.2017.259.

Lawson, C., D. Kovacs, E. Finding, E. Ulfelder, and V. Luis-Fuentes. 2017. "Extracellular Vesicles: Evolutionarily Conserved Mediators of Intercellular Communication." *Yale Journal of Biology and Medicine* 90: 481–491.

Liu, Y., S. E. Elf, Y. Miyata, et al. 2009. "p53 Regulates Hematopoietic Stem Cell Quiescence." *Cell Stem Cell* 4: 37–48. https://doi.org/10.1016/j.stem.2008.11.006.

Majeti, R., C. Y. Park, and I. L. Weissman. 2007. "Identification of a Hierarchy of Multipotent Hematopoietic Progenitors in Human Cord Blood." *Cell Stem Cell* 1: 635–645. https://doi.org/10.1016/j.stem.2007.10.001.

Manz, M. G., T. Miyamoto, K. Akashi, and I. L. Weissman. 2002. "Prospective Isolation of Human Clonogenic Common Myeloid Progenitors." *PNAS* 99: 11872–11877. https://doi.org/10.1073/pnas.172384399.

McCulloch, E. A., T. W. Mak, G. B. Price, and J. E. Till. 1974. "Organization and Communication in Populations of Normal and Leukemic Hemopoietic Cells." *Biochimica Et Biophysica Acta* 355: 260–299. https://doi.org/10.1016/0304-419x(74)90013-4.

Mendelson, A., and P. S. Frenette. 2014. "Hematopoietic Stem Cell Niche Maintenance During Homeostasis and Regeneration." *Nature Medicine* 20: 833–846. https://doi.org/10.1038/nm.3647.

Morrison, S. J., and D. T. Scadden. 2014. "The Bone Marrow Niche for Haematopoietic Stem Cells." *Nature* 505: 327–334. https://doi.org/10.1038/nature12984.

Njock, M. S., T. O'Grady, O. Nivelles, et al. 2022. "Endothelial Extracellular Vesicles Promote Tumour Growth by Tumour-Associated Macrophage Reprogramming." *Journal of Extracellular Vesicles* 11: e12228. https://doi.org/10.1002/jev2.12228.

Noubouossie, D. F., and N. S. Key. 2023. "Red Cell Extracellular Vesicles and Coagulation Activation Pathways." *Current Opinion in Hematology* 30: 194–202. https://doi.org/10.1097/MOH.0000000000000780.

Paggetti, J., F. Haderk, M. Seiffert, et al. 2015. "Exosomes Released by Chronic Lymphocytic Leukemia Cells Induce the Transition of Stromal Cells Into Cancer-Associated Fibroblasts." *Blood* 126: 1106–1117. https://doi.org/10.1182/blood-2014-12-618025.

Panarelli, N., K. Tyryshkin, J. J. M. Wong, et al. 2019. "Evaluating Gastroenteropancreatic Neuroendocrine Tumors Through microRNA Sequencing." *Endocrine-Related Cancer* 26: 47–57. https://doi.org/10.1530/ERC-18-0244.

Parker, R. S. 1989. "Carotenoids in Human Blood and Tissues." *Journal of Nutrition* 119: 101–104. https://doi.org/10.1093/jn/119.1.101.

Peinado, H., M. Alečković, S. Lavotshkin, et al. 2012. "Melanoma Exosomes Educate Bone Marrow Progenitor Cells Toward a Pro-Metastatic Phenotype Through MET." *Nature Medicine* 18: 883–891. https://doi.org/10.1038/nm.2753.

Penders, J., A. Nagelkerke, E. M. Cunnane, et al. 2021. "Single Particle Automated Raman Trapping Analysis of Breast Cancer Cell-Derived Extracellular Vesicles as Cancer Biomarkers." *ACS Nano* 15: 18192–18205. https://doi.org/10.1021/acsnano.1c07075.

Penders, J., I. J. Pence, C. C. Horgan, et al. 2018. "Single Particle Automated Raman Trapping Analysis." *Nature Communications* 9: 4256. https://doi.org/10.1038/s41467-018-06397-6.

Peng, M., J. Ren, Y. Jing, et al. 2021. "Tumour-Derived Small Extracellular Vesicles Suppress CD8+ T Cell Immune Function by Inhibiting SLC6A8-Mediated Creatine Import in NPM1-Mutated Acute Myeloid Leukaemia." *Journal of Extracellular Vesicles* 10: e12168. https://doi.org/10.1002/jev2.12168.

Pietras, E. M., D. Reynaud, Y.-A. Kang, et al. 2015. "Functionally Distinct Subsets of Lineage-Biased Multipotent Progenitors Control Blood Production in Normal and Regenerative Conditions." *Cell Stem Cell* 17: 35–46. https://doi.org/10.1016/j.stem.2015.05.003.

Pinho, S., and P. S. Frenette. 2019. "Haematopoietic Stem Cell Activity and Interactions With the Niche." *Nature Reviews Molecular Cell Biology* 20: 303–320. https://doi.org/10.1038/s41580-019-0103-9.

Reimand, J., R. Isserlin, V. Voisin, et al. 2019. "Pathway Enrichment Analysis and Visualization of Omics Data Using G:Profiler, GSEA, Cytoscape and EnrichmentMap." *Nature Protocols* 14: 482–517. https://doi.org/10.1038/s41596-018-0103-9.

Reimand, J., M. Kull, H. Peterson, J. Hansen, and J. Vilo. 2007. "g:Profiler—A Web-Based Toolset for Functional Profiling of Gene Lists From Large-Scale Experiments." *Nucleic Acids Research* 35: W193–W200. https://doi.org/10.1093/nar/gkm226.

Sawai, C. M., S. Babovic, S. Upadhaya, et al. 2016. "Hematopoietic Stem Cells Are the Major Source of Multilineage Hematopoiesis in Adult Animals." *Immunity* 45: 597–609. https://doi.org/10.1016/j.immuni.2016.08.007.

Shu, S., Y. Yang, C. L. Allen, et al. 2018. "Metabolic Reprogramming of Stromal Fibroblasts by Melanoma Exosome microRNA Favours a Pre-Metastatic Microenvironment." *Scientific Reports* 8: 12905. https://doi.org/10.1038/s41598-018-31323-7.

Simon, C., D. W. Greening, D. Bolumar, N. Balaguer, L. A. Salamonsen, and F. Vilella. 2018. "Extracellular Vesicles in Human Reproduction in Health and Disease." *Endocrine Reviews* 39: 292–332. https://doi.org/10.1210/er.2017-00229.

Todorova, D., S. Simoncini, R. Lacroix, F. Sabatier, and F. Dignat-George. 2017. "Extracellular Vesicles in Angiogenesis." *Circulation Research* 120: 1658–1673. https://doi.org/10.1161/CIRCRESAHA.117.309681.

Traber, M. G., S. R. Diamond, J. C. Lane, R. I. Brody, and H. J. Kayden. 1994. "Beta-Carotene Transport in Human Lipoproteins. Comparisons With a Tocopherol." *Lipids* 29: 665–669. https://doi.org/10.1007/BF02538909.

van Niel, G., G. D'Angelo, and G. Raposo. 2018. "Shedding Light on the Cell Biology of Extracellular Vesicles." *Nature Reviews Molecular Cell Biology* 19: 213–228. https://doi.org/10.1038/nrm.2017.125.

Verovskaya, E. V., P. V. Dellorusso, and E. Passegué. 2019. "Losing Sense of Self and Surroundings: Hematopoietic Stem Cell Aging and Leukemic Transformation." *Trends in Molecular Medicine* 25: 494–515. https://doi.org/10.1016/j.molmed.2019.04.006.

Wang, G., J. Li, L. Bojmar, et al. 2023. "Tumour Extracellular Vesicles and Particles Induce Liver Metabolic Dysfunction." *Nature* 618: 374–382. https://doi.org/10.1038/s41586-023-06114-4.

Watson, E. C., and R. H. Adams. 2018. "Biology of Bone: The Vasculature of the Skeletal System." *Cold Spring Harbor Perspectives in Medicine* 8: a031559. https://doi.org/10.1101/cshperspect.a031559.

Wattrus, S. J., and L. I. Zon. 2018. "Stem Cell Safe Harbor: The Hematopoietic Stem Cell Niche in Zebrafish." *Blood Advances* 2: 3063–3069. https://doi.org/10.1182/bloodadvances.2018021725.

Wei, Q., and P. S. Frenette. 2018. "Niches for Hematopoietic Stem Cells and Their Progeny." *Immunity* 48: 632–648. https://doi.org/10.1016/j.immuni.2018.03.024.

Wells, C. J., et al. 2025. Enriching for Extracellular Vesicles from Human Bone. *bioRxiv* 2025.2006.2018.660234. https://doi.org/10.1101/2025.06.18.660234.

Welsh, J. A., D. C. I. Goberdhan, L. O'Driscoll, et al. 2024. "Minimal Information for Studies of Extracellular Vesicles (MISEV2023): From Basic to Advanced Approaches." *Journal of Extracellular Vesicles* 13: e12404. https://doi.org/10.1002/jev2.12404.

Supporting Information

Additional supporting information can be found online in the Supporting Information section.

Supplementary Materials: jev270181-sup-0001-SuppMat.pdf **Supplementary Tables**: jev270181-sup-0001-TableS1-S10.xlsx